

Muscular morphometric study of the canine shoulder for the design of 3D-printed endoprostheses in dogs with osteosarcoma of the proximal humerus: a pilot cadaveric study by MRI

Marie Llido, DVM^{1*}; Linh-Aurore Le Bras, MS²; Vladimir Brailovski, PhD²; Bernard Séguin, DACVS³; Isabelle Masseur, DACVD¹; Yvan Petit, PhD²; Bertrand Lussier, DACVS¹

¹Department of Sciences Cliniques, Faculty of Veterinary Medicine, University of Montreal, St-Hyacinthe, Quebec, Canada

²École de Technologie Supérieure, Montreal, Quebec, Canada

³Central Victoria Veterinary Hospital, Victoria, British Columbia, Canada

*Corresponding author: Dr. Llido (llido.marie@gmail.com)

Received December 24, 2022

Accepted March 15, 2023

doi.org/10.2460/ajvr.22.12.0220

© 2023 THE AUTHORS. Published by the American Veterinary Medical Association

OBJECTIVE

Osteosarcoma frequently affects the proximal humerus in dogs. In veterinary medicine, no therapeutic option for the treatment of osteosarcoma satisfactorily preserves limb function. 3D-printed personalized endoprosthesis offers a promising treatment option. Morphometric data, necessary for the design of the endoprosthesis, are currently lacking in canine patients. Our objective was to acquire the morphometric data necessary to refine the design of the endoprosthesis.

ANIMAL

A single canine cadaveric thoracic limb.

PROCEDURES

Sagittal proton-density, and sagittal, dorsal, and transverse T1-weighted sequences of the thoracic limb were acquired with a 1.5 Tesla Magnetic Resonance Imaging (MRI) unit. Nineteen muscles of interest were subsequently identified using medical imaging software (Mimics©) and their volume was reconstructed in 3D using computer-aided design (CATIA©). Morphometric data were recorded for each of the 19 muscles. The same canine cadaver was then dissected to measure the same parameters.

RESULTS

All muscles were successfully identified with data consistent with the dissected cadaveric data. Certain muscles were more challenging to isolate on MRI, namely the heads of the triceps brachii, superficial pectoral, and latissimus dorsi. The relative distribution of muscle volumes was similar to historical data. Muscle tissue density was not significantly affected by freezing (1.059 g/cm³).

CLINICAL RELEVANCE

MRI is a useful tool to collect morphometric data but imperfect if used alone. This approach was the first attempt to validate more general morphometric data that could be used to refine the design of custom 3D-printed prostheses for limb-sparing of the proximal humerus. Further imaging studies are warranted to refine our model.

Between 10 000 to 45 000 dogs develop osteosarcoma (OSA) each year in the United States.^{1,2} The proximal humerus is one of the most common anatomic sites for appendicular OSA with a prevalence as high as 20.9%.³ Although amputation arguably remains the standard of care for primary tumor treatment, some dogs are not ideal candidates due to concurrent orthopedic or neurologic diseases. Furthermore, amputation can also lead to some negative sequelae such as changes in behavior, aggression, and anxiety.^{4,5} Treatment alternatives include surgical limb-sparing

using an allograft, intra-operative radiation therapy, and stereotactic radiation therapy (SRT). The use of an allograft for the proximal humerus has been associated with a high complication rate and poor limb function.⁶ Intraoperative radiation therapy in dogs afflicted with humeral osteosarcoma led to complications in all dogs of a study, including fracture, implant failure, infection, and radial nerve paralysis.⁷ The most common major complication associated with SRT is a fracture.^{8,9} Therefore, there are currently no limb-sparing options for proximal humeral osteosarcoma

with an acceptable risk of complications. In human medicine, patient-specific implants are engineered to fit as perfectly as possible to each patient; thereby, optimizing the loads transmitted through the limb.^{10,11} Patient-specific implants are possible through computer-aided design and additive manufacturing also known as 3D printing and have been used for the treatment of dogs with appendicular osteosarcomas.^{12,13} Three different designs of limb-sparing endoprostheses for the canine proximal humerus are conceptually possible including the arthrodesis, the 1 degree of liberty (flexion-extension), and the full range of motion. When mobility is introduced, active stabilization becomes crucial for the functionality of the endoprosthesis. Based on this assumption, the relative importance of the shoulder muscles is imperative to consider. However, relevant morphometric data on the thoracic limb in dogs are lacking. The objective of our study was to acquire morphometric data on the shoulder muscles and compare them to historical data previously described in cadavers by Shahar et al.¹⁴

Materials and Methods

Specimen selection

The left thoracic limb was collected from a mature dog euthanized for reason unrelated to this study. The limb was retrieved following the harvest of other organs by other investigators for research and teaching purposes in accordance with the 3R rules by Russell and Burch.¹⁵ No approval from our IACUC was required. The mesomorphic-type dog weighed 30 kg and was a male mixed breed. This dog had a body condition score of 5 out of 9 based on the scale developed by Laflamme et al.¹⁶ and a muscle condition score of 3 based on the scale developed by the World Small Animal Veterinary Association (WSAVA).¹⁷ Macroscopic examination and palpation of the thoracic limb joints were performed by a surgeon (ACVS diplomate) to rule out any gross abnormalities (eg, malformation, instability, and crepitus). The entire cadaver was frozen at -20°C until specimen preparation.

Specimen preparation

Before preparation, the cadaver was thawed at 4°C for 48 hours. Then, the left thoracic limb and the left part of the thoracic wall including all of the left ribs were isolated from the remainder of the cadaver with an oscillating saw dividing the sternum in half, for the dorsal aspect of the ribs were transected from the spine at their insertion with a bone cutter. To optimize MRI image acquisition, the limb was sawed mid-radius.

MRI study

MRI (1.5 Tesla magnet GE Signa Echospeed HDx; GE Healthcare) of the thoracic limb and left part of the thoracic wall was performed extending from the most proximo-caudal tip of the scapula to the proximal third of the radius or ulna. The study included the following sequences: sagittal proton-density (PD), and sagittal, dorsal, and transverse T1-weighted

fast spin echo using a torso coil. The reduction in the size of the specimen allowed for use of a relatively small field of view (sagittal PD, T1, FIESTA: 26 cm; Trans FIESTA: 16 cm; Trans T1: 17 cm), optimizing the spatial resolution and increasing the signal-to-noise ratio (SNR). The shoulder was positioned at 130° and the elbow at 130° , to mimic the standard standing position.¹⁸⁻²⁰ As previously described in the specimen preparation, MRI included the left thoracic wall, scapula, humerus, and proximal part of the radius and ulna.

Morphometric data acquisition on MRI sequences

The MRI sequences were treated with medical imaging software (Mimics©, research 19.0 Materialise). An MRI sequence was selected, providing the best visualization of the muscle studied and treated as a multiplanar reconstruction with 3 different views simultaneously available (coronal, sagittal, and transverse). The different axis system bases were defined in the axis system of the software based on previously described landmarks.¹⁴ To complete an associated ongoing study,²¹ coordinates of the scapula- and humerus-based axis systems, rotation center between the scapula and humerus, and rotation center between the humerus and the radius were recorded by the coordinates of the point of interest searched in the 3 different planes (transverse, longitudinal, and coronal) by 1 investigator (M.L.). The following 19 muscles were individually studied: deep pectoral, superficial descending pectoral, superficial transversus pectoral, supraspinatus, infraspinatus, teres major, teres minor, deltoid – acromial part, deltoid – scapular part, triceps brachii – accessory head, triceps brachii – long head, triceps brachii – medial head, triceps brachii – lateral head, biceps brachii, subscapularis, latissimus dorsi, coracobrachialis, brachiocephalicus, brachialis. Those muscles of interest were chosen because they are responsible for shoulder motion and may be damaged during the removal of humeral osteosarcoma or reattachment in case of endoprosthesis placement afterward. The following morphometric data were recorded for each muscle: coordinates of insertion and origin points, maximal length including tendon, maximal cross-section area, and volume. Insertion and origin points of each muscle were located in the 3 planes (transverse, longitudinal, and coronal) based on anatomic landmarks and MRI sequences; the tendon part was considered part of the muscle. The origin point was marked with a cursor on the MRI images, allowing visual assessment and record of coordinates. The same process was repeated for the insertion point. To determine the length of a muscle, the origin and insertion points were linked with the distance measure function and the length of the muscle in centimeters (cm) was recorded. To define the volume of the muscle, a plane was chosen based on the best visualization of the muscle, either transverse, sagittal, or dorsal. The surface area of the muscle was defined by tracing the perimeter of the chosen muscle section on the selected layer and plane, the

perimeter of the muscle section was then defined on each consecutive layer on the same previously selected plane. The surface area on each image was then summed up to create an STL volume, as presented (**Figure 1**). This STL file was then transferred into software for computer-aided design (CATIA© V5 Dassault Systemes) to generate a 3D reconstruction of the muscle and determine the volume in cubic centimeters as presented (**Figure 2**). This image treatment was performed by 1 investigator (L.L.B.). The maximal cross-section area was defined as the maximal surface area drawn for each muscle in square centimeters. Data collection was validated by a board-certified veterinary radiologist (I.M.).

Cadaveric study

Following MRI acquisition, the same cadaveric specimen was then dissected to isolate the 19 muscles of interest. For each muscle, the following data were recorded: volume, maximal length, maximal cross-section area, and muscle tissue density. First, the volume in cubic centimeters was measured using Archimedes' principle. This principle states that when a body is (partially or totally) immersed in a fluid, the upthrust on the body is equal to the weight of the fluid displaced. Each measurement was done in triplicate by 1 investigator (M.L.). The muscle was then placed on a flat surface and a ruler was used to measure the length from the origin of the muscle to its insertion, 1 investigator (M.L.) as previously described by Shahar.¹⁴ Tendons were included in the total length of the muscle. Each measurement was done in triplicate. The maximal cross-section area was subjectively assessed by 2 observers (B.L., M.L.). To do this, a section of the muscle was cut, then a

metal ruler was used for calibration, and placed next to it. A photograph was taken after placing the camera perpendicular to the surface, as shown (**Figure 3**). Each photograph was repeated 3 times. The photographic image was treated with planimetry freeware (Fiji©) based on previous studies describing it for laryngeal glottis measurements²² or wound healing granulation and contraction assessment.²³ Each image was first calibrated, using the metal ruler included in the photograph. The outline of the muscle was then traced by 1 investigator (M.L.) to determine the perimeter of the muscle surface and the software generated the measured surface area in square centimeters. This procedure was repeated for each image and each muscle in triplicate to improve precision. Three 1-cm³ cubes of muscle were then weighted. The volumetric mass density in grams per cubic centimeters was, therefore, determined. Data collection was validated by a board-certified veterinary surgeon (B.L.).

Data analysis

The different data were quantitatively compared as described between the 3 scenarios: MRI data, cadaveric data, and historical data from Shahar.¹⁴ Due to the nature of this pilot study only 1 measurement per method was available to compare; therefore, no statistical test could be performed to compare methods for a single muscle at a time. The authors chose to calculate for each measurement the percentage of error between methods (modelization vs cadaver, modelization vs historical data, and cadaver vs historical data). Subjectively when the difference was below 40% the value was considered comparable or consistent. Then we wanted to

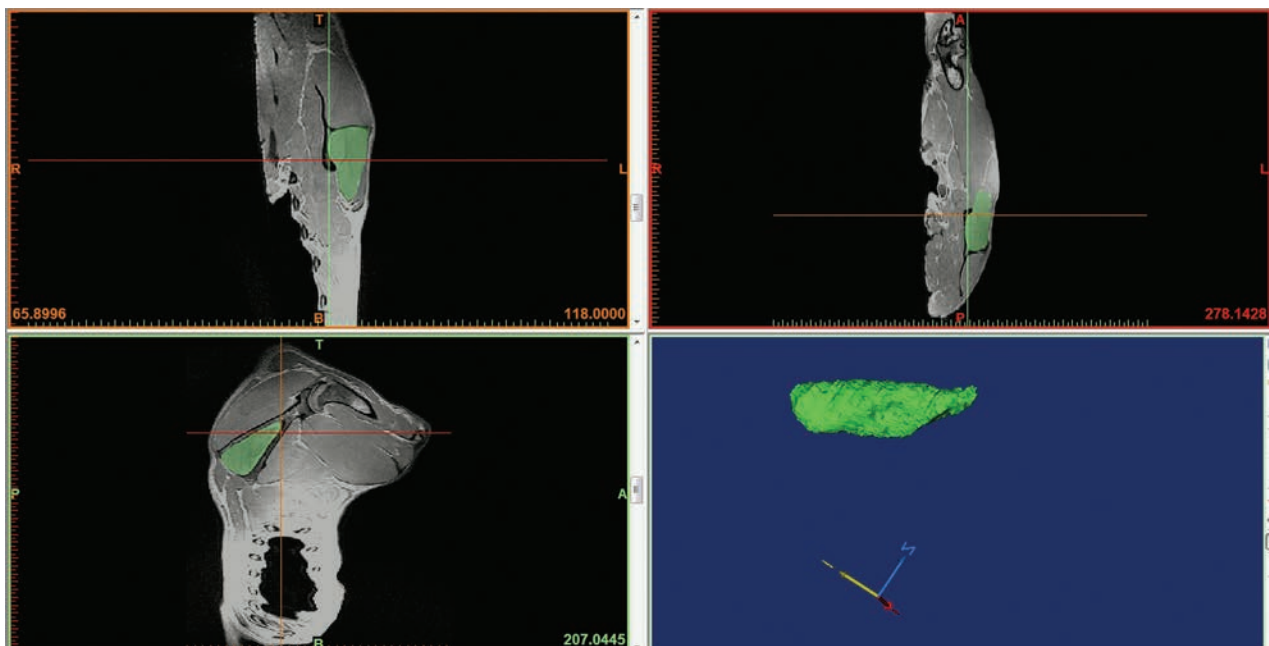


Figure 1—Identification of the muscles of interest using medical imaging software (Mimics) after magnetic resonance imaging of the proximal aspect of a canine thoracic limb. The *infraspinatus* muscle is identified in green on the dorsal (A), sagittal (B), and transverse (C) images. The 3D-volume rendering on the muscle, used to generate the .stl file, is shown in D.

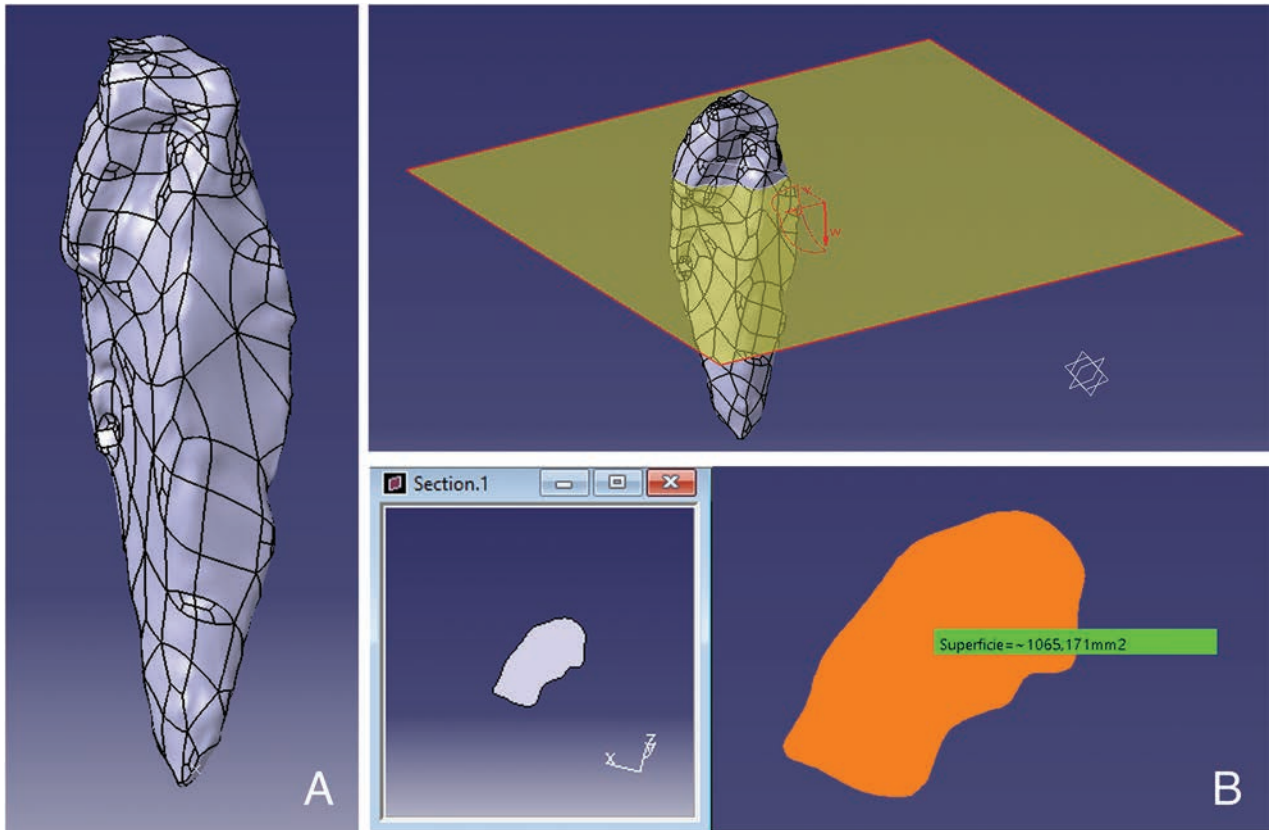


Figure 2—Volume reconstruction (A) and maximal surface area (B) determination of the *supraspinatus* muscle in computer-aided design software (Catia, Dassault Systems©)

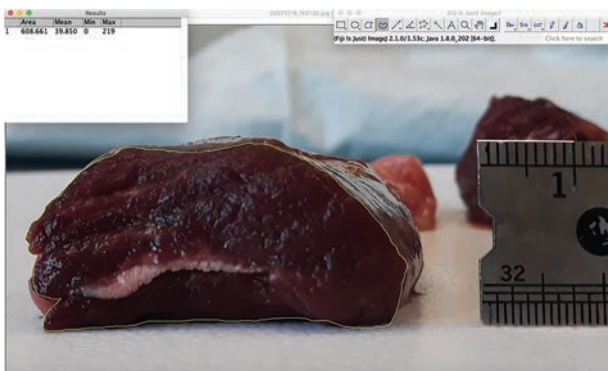


Figure 3—Example of a photographic image of the *biceps brachii* muscle used for computerized planimetric analysis with Fiji© software. A metallic ruler is placed next to the muscle cross-section to allow for calibration and for the determination of the maximal surface area.

compare methods of measurement for each parameter (maximal length, maximal cross-section area, volume, mass of the muscle, and relative volume). We hypothesized that our measurement for each parameter was a repeated measure of the same muscle in an identical dog, our variables were continuous, and we had a small sample size. Based on all of these criteria we elected to perform an intra-class correlation coefficient (ICC) to determine the concordance between our 3 methods of evaluation. This

coefficient can take a value between 0 and 1, with 0 indicating no agreement and 1 indicating perfect agreement. When comparing the data the authors used the study of Koo et al.²⁴ to interpret the ICC. The ICC values below 0.5 indicate poor reliability, between 0.5 and 0.75 moderate reliability, between 0.75 and 0.9 good reliability, and any value above 0.9 indicates excellent reliability. When the authors are using the terms similar or consistent it is for good or excellent reliability, with ICC above 0.75.

Results

All data are summarized (**Table 1**). All muscles were successfully identified on MRI images, and reconstructed in their respective 3D shapes. The maximal lengths of the muscles obtained from the MRI and the cadaver were consistent for the majority of the muscles (17/19) of interest. The maximal section areas were consistent for 18/19 of the muscles. The volume obtained from 3D reconstruction and the cadaver was consistent for 14/19 muscles of interest. Indeed, some muscles were more challenging to isolate on MRI sequences, namely the individual heads of the triceps brachii, the superficial pectoral, the teres minor, and the latissimus dorsi. The volumes of the muscles' specimens in this study were more substantial than the historical data.¹⁴ To overcome the fact that dogs used for historical data and in our

Table 1—Comparison of morphometric data for each of the 19 muscles of interest between modelization by magnetic resonance imaging (MOD), cadaver (CAD), and historical data (HD). The muscle mass of historical data was determined by calculation with a gravity of 1.059 g/cm³.

Muscle	Maximal length (cm)			Maximal cross-section area (cm ²)		Volume (cm ³)			Mass of the whole muscle (g)		
	MOD	CAD	HD	MOD	CAD	MOD	CAD	HD	MOD	CAD	HD
Biceps brachii	14.65	15.6	11.05	5.24	6.17	36.68	48	26.36	38.84	49.03	27.92
Brachialis	11.61	13.4	13.45	3.11	3.21	17.70	22	14.6	18.75	24.27	15.46
Brachiocephalicus	10.19	13.6	34.89	3.77	2.25	17.00	18	50.65	18.01	18.83	53.64
Coracobrachialis	4.65	7.5	5.38	1.65	1.44	5.56	5	3.02	5.89	5.2	3.2
Deltoid – acromial part	8.58	8.1	7.5	3.91	4.78	24.79	24	13.4	26.26	24.78	14.19
Deltoid – scapular part	9.88	14.7	11.25	3.61	4.22	20.97	42	20.59	22.21	43.34	21.81
Infraspinatus	14.92	17.3	14.13	9.11	9.16	76.43	100	57.18	80.94	90.66	60.55
Latissimus dorsi	22.92	27.3	29.38	14.13	19.99	152.87	305	140.02	161.89	304.62	148.28
Deep pectoral	20.09	23.0	23.28	13.06	10.23	199.4	190	153.59	211.16	176.35	162.65
Superficial descending pectoral	14.21	18.8	10.75	5.52	4.30	34.32	39	12.47	36.34	40.56	13.21
Superficial transversus pectoral	15.41	10.8	8.55	10.26	7.83	51.57	62	39.19	54.61	65.5	41.5
Subscapularis	12.25	12.8	11.1	7.17	9.72	37.72	62	48.46	39.95	65.48	51.32
Supraspinatus	16.14	16.8	15.08	12.27	16.06	107	160	75.37	139.05	113.31	79.82
Teres minor	5.79	9.6	4.98	2.44	2.16	5.03	7	3.79	5.32	7.73	4.01
Teres major	12.82	17.3	14.08	5.24	4.51	22.75	45	28.87	24.09	47.3	30.57
Triceps brachii – accessory head	4.86	14.0	11.13	4.14	4.30	12.05	25	20.44	12.05	27.92	21.65
Triceps brachii – long head	17.71	17.1	15.35	26.15	23.52	358.71	300	140.46	379.87	271.42	148.75
Triceps brachii – medial head	11.04	12.7	11.28	2.94	4.80	9.90	30	22.83	10.49	33.03	24.18
Triceps brachii – lateral head	11.86	12.8	12	5.71	7.92	45.02	70	48.32	47.67	74.56	51.17

Table 2—A posteriori analysis of the relative volume of the 19 muscles of interest.

Muscle	Relative volume (%)		
	Modelization	Cadaver	Historical data
Biceps brachii	3	3.1	2.9
Brachialis	1.4	1.4	1.6
Brachiocephalicus	1.4	1.2	5.5
Coracobrachialis	0.5	0.3	0.3
Deltoid – acromial part	2	1.5	1.5
Deltoid – scapular part	1.7	2.7	2.2
Infraspinatus	6.2	6.4	6.2
Latissimus dorsi	12.4	19.6	15.2
Deep pectoral	16.1	12.2	16.7
Superficial descending pectoral	2.8	2.5	1.4
Superficial transversus pectoral	4.2	4	4.3
Subscapularis	3.1	4	5.3
Supraspinatus	8.7	10.3	8.2
Teres minor	0.4	0.5	0.4
Teres major	1.8	2.9	3.1
Triceps brachii – accessory head	1	1.6	2.2
Triceps brachii – long head	28.9	19.4	15.2
Triceps brachii – medial head	0.8	1.9	2.5
Triceps brachii – lateral head	3.6	4.5	5.3
Total	100	100	100

study had different weights, a posteriori analysis was performed and relative repartition of the muscle volume was calculated. The results of this analysis are summarized (**Table 2**). This relative repartition was similar for 17/19 of the muscles. Overall, the muscle tissue density was not significantly different from the reference value,²⁵ known as 1.059 g/cm³. The agreement between methods of measurement was considered excellent (ICC > 0.90) for maximal cross-section area (modelization vs cadaver) and relative volume (modelization vs cadaver, historical data vs cadaver). It was considered good (0.75 < ICC < 0.9) for maximal length (modelization vs cadaver), volume (modelization vs cadaver, modelization vs historical data), mass (modelization vs cadaver, modelization vs historical data), and relative volume (modelization vs historical data). It was considered moderate (0.5 < ICC < 0.75) for the remaining comparison.

Discussion

This pilot study allowed the identification of the 19 muscles of interest in the canine shoulder with MRI and medical imaging software. The morphometric data collected with imaging proved to be consistent with those obtained by dissection and with historical data. Volume reconstruction was performed for the 19 muscles with the software for computer-aided design. Dissection and measurements of the different variables were successfully performed for all muscles of interest without any complication. A posteriori analysis provided evidence that mesomorphic dogs

may have a similar relative muscle volume repartition. Our study also provides supporting evidence that muscle density is not affected by freezing and a reference value²⁵ of 1.059 g/cm³ can be used safely.

Precise identification on MRI of each muscle had to overcome several obstacles. First, different heads of the triceps brachii were difficult to isolate from each other despite attempts to optimize the MRI sequence acquisition. To overcome this difficulty, additional sequences such as T2-FLAIR might have been useful to isolate each head and distinguish between muscle and fat. Second, an MRI of superior quality could be useful (3 Tesla),²⁶ or sequential acquisition could be performed.²⁷ In human medicine MRI of the superior quality previously mentioned provides sufficient quality to identify muscle fibers.²⁶ Third, identification of the latissimus dorsi muscle would have benefited from increased resolution due to its multiple fibers that are tedious to identify. Finally, the pre-treatment (ie, thoracic cavity transected on the medial plane) and positioning of the cadaver may have introduced some distortion of the muscles. Indeed, the specimen was positioned lying on its side during the image acquisition. This position may have modified the anatomic position of the superficial pectoral (descending and transversus) and rendering its identification more tedious. In a living dog, a dorsal recumbency would be preferred and has been described for the detection of muscular dystrophy by MRI.²⁸

Despite imperfections, the MRI allowed the identification of 19 muscles of interest, an essential step for subsequent 3-D volume rendering by software for computer-aided design, and measurement of volume was successfully obtained for each of them. The acquisition of sequential tracing for each layer of each muscle was performed by 1 investigator. This acquisition was time-consuming, especially knowing that no pre-settings were available to identify muscle fibers on the software. This study is the first attempt to describe a step-by-step methodology to identify canine shoulder muscles on MRI images. The end goal would be to automatize the process with machine learning techniques to mimic what is currently done in human medicine.²⁶ However, it would require a better definition to create reliable algorithms of identification.

Selected morphometric data was successfully acquired using MRI and the previously described software for volume, maximal length including tendon, and maximal cross-section area. The latter 2 parameters were measured to assess in which plane the error could have been made in the event of volume discrepancy between the gold standard (dissection) and modelization. The agreement between modelization with the MRI and cadaver measurements was greater for maximal cross-section area measurement (ICC 0.93) compared with maximal length (ICC 0.75). It means that error may be more related to the difficulty in assessing the origin and insertion of the muscle (maximal length) rather than missing fibers in the belly of the muscle (maximal cross-section area). The importance to

identifying the source of the error was particularly important to refine the technique. Fourteen out of 19 muscles had a comparable volume between modelization and dissection, meaning less than a 40% difference in the data between the methods used to do the measurement. Some discrepancy remained for the accessory and medial heads of the triceps brachii that could be related to a difficult distinction on the MRI images of the heads of this muscle. As previously discussed, additional MRI sequences such as T2-Flair should be planned in future studies. The discrepancy in volume was also present for the latissimus dorsi when comparing modelization and cadaver data. This could be secondary to failing to identify some fibers of this muscle on the MRI images due to the subtlety of some fibers that may have been missed with distortion and lack of adequate definition. This discrepancy can also be secondary to the loss of tendinous attachments in the process of specimen preparation, which could make identification of the origin of the muscle more difficult. When comparing the volume of muscles with historical data,¹⁴ all muscles except for the brachiocephalicus, were larger in our specimen. The dog used in the study weighed 30 kg compared with a mean of 20 kg for the historical data. To overcome this discrepancy, we elected to perform a posteriori analysis of our results and calculate relative volume repartition. This analysis showed that the relative volume repartition between the different muscles seemed to be similar in the mesomorphic dogs included in this study and in historical data.¹⁴ This is a promising result that could be used in the future if proven to be generalized to all mesomorphic dogs. As a result, a simple algorithm could be used to obtain each muscle volume knowing the body condition score¹⁶ and weight of a mesomorphic dog. Further research is needed to verify this hypothesis and to assess relative muscle volume repartition for each type of dog. Some data available for greyhounds could not be extrapolated to our results due to morphology discrepancy.²⁹ The maximal length was comparable for the majority of muscles between the modelization and the cadaver with the exception of the superficial pectoral (transversus), which could be due to positioning and limited delineation of the accessory head of the triceps brachii resulting from a poor definition on selected MRI sequences. Moreover, the definition was not always adequate, and tendons were sometimes difficult to identify for all the muscles.

A comparison of the maximal length with the historical data revealed a tendency to be longer in our specimen compared with the historical data, which is consistent with our specimen being heavier and likely taller. The maximal surface area was also comparable for the majority of muscles, with the exception of the medial head of the triceps brachii and the latissimus dorsi, which would be related to a misidentification of the entire perimeter of the muscle.

Our study provides new morphometric data of the canine shoulder muscles acquired by a non-invasive method; however, with this imaging method alone, some morphometric data are lacking. Some

parameters such as pennation angle and muscle fiber length are missing in our study to have a complete muscle evaluation in his composition and geometry. Those parameters were not possible to acquire due to technical limitations such as insufficient definition and lack of fiber enhancement. Muscle fiber distribution in concordance with the volume of the muscle dictates the amount of force that can be generated by a muscle during locomotion.³⁰ Muscle fibers' length and orientation have been shown in a recent study³¹ to influence the direction of the force generated by the muscle. Each muscle can be defined by a specific type of morphology³² (ie, parallel, unipennate, bipennate, or circular). The orientation of muscle fibers is usually defined by the pennation angle³³ used to calculate the physiological cross-sectional area (PCSA). Ultrasound has been described³⁴ to measure the pennation angle of muscles and it would have been interesting to pair sonographic measures of the pennation angle with MRI and define each muscle morphology based on both modalities. Measurement of the pennation angle has been described in human medicine with advanced definition MRI (3-Tesla)²⁶ and was not possible with our images.

Our pilot study provides evidence that the identification of canine shoulder muscles by MRI is feasible. The goal of this study is not to replace the large dissection textbooks but rather to provide complementary evidence to understand shoulder muscle volume repartition. The muscle volume is correlated with the force generated by its contraction.³⁰ By understanding the relative contribution of each muscle, we could then calculate the resulting forces that will be generated on different types of endoprostheses. This information is pivotal in creating endoprostheses that will withstand daily weight bearing in dogs that had undergone proximal humeral limb-sparing surgery. Moreover, the use of this imaging modality allowed a 3D evaluation of muscle and in cases of osteosarcoma could refine the pre-planning of the endoprosthesis. The end goal of this technique is to acquire morphometric data with machine learning tools and automatize the process. Transitioning from this pilot study to live animals could be done first by repetition of the same acquisition on various morphotypes of dogs to create an algorithm to identify reliably the muscles. The same study could try to validate the hypothesis that the relative volume of canine shoulder muscle may be similar in mesomorphic dogs. It is expected that ectomorphic and endomorphic dogs may have different repartition of muscle. To address this question those morphometric data could be used in a mathematical algorithm to assess the contribution of each muscle to the shoulder function.²¹ To use such type of algorithm fixed landmarks should be defined on the limb with software. The identification of the most important muscles and their impact on the kinematics of the prosthetic joint will then lead to improved endoprosthesis design and implantation feasibility. Understanding which muscles are crucial to reimplant and which ones could be sacrificed during dissection would reduce surgery time and improve

endoprosthesis stability by shoulder muscles. Based on this technique the surgical approach could be adapted for every type of dog conformation and address the difference in muscle morphology by breed. Furthermore, precise identification of muscle can lead to location choice for lattices that will allow tendinous reimplantation for muscle that should absolutely be salvaged during the procedure to allow a successful function. The authors believe that this field of work could be promising with the appropriate understanding of muscles' contribution during locomotion to create personalized endoprosthesis in cases of proximal humeral osteosarcoma.

This pilot study encountered some limitations, the main one being the use of a thoracic limb of a single individual. This precludes the generalization of the method but has served to highlight several possible solutions to refine the technique, which was the goal of this pilot study. Indeed, a single individual has prevented any statistical analysis of the repeatability of the modelization or identification of various individual factors that can affect the accuracy of measurements (body condition score, muscle condition score, morphotype, and breed). The limb was severed at the proximal radius and muscles attaching distally to this section were not included in our research. Further studies should include the entire limb to collect complete morphometric data of the thoracic limb and allow the development of more complex and accurate models.

This pilot study was the first attempt toward validation of a more general method for acquiring morphometric data of the muscles of the canine proximal thoracic limb. While MRI has proven to be a useful tool to collect morphometric data, it remains imperfect when used alone. A posteriori analysis provided evidence that mesomorphic dogs may have a similar relative muscle volume repartition. The generalization of this conclusion remains to be proven. Further imaging studies are warranted to refine the model before applying it to prosthetic design.

Acknowledgments

This project was funded by the ÉTS Laboratory on Shape Memory and Intelligent systems (V.B.), Canada Research Chair in Biomechanics of Head and Spine Trauma (Y.P.), and the University of Montreal internal funds (B.L.).

References

1. Ehrhart N. Tumors of the skeletal system. In: *Withrow and MacEwen's Small Animal Clinical Oncology*. 6th ed. Elsevier; 2020:842.
2. Mason NJ. Comparative immunology and immunotherapy of canine osteosarcoma. In: Kleinerman ES, Gorlick R, eds. *Current Advances in the Science of Osteosarcoma. Advances in Experimental Medicine and Biology, Vol 1258*. Springer International Publishing; 2020: 199–221. doi:10.1007/978-3-030-43085-6_14
3. Tuohy JL, Shaevitz MH, Garrett LD, Ruple A, Selmic LE. Demographic characteristics, site and phylogenetic distribution of dogs with appendicular osteosarcoma: 744 dogs (2000–2015). *PLoS ONE*. 2019;14(12):e0223243. doi:10.1371/journal.pone.0223243

4. Kirpensteijn J, van den Bos R, Enderburg N. Adaptation of dogs to the amputation of a limb and their owners' satisfaction with the procedure. *Vet Rec.* 1999;144(5):115-118. doi:10.1136/vr.144.5.115
5. Dickerson VM, Coleman KD, Ogawa M, et al. Outcomes of dogs undergoing limb amputation, owner satisfaction with limb amputation procedures, and owner perceptions regarding postsurgical adaptation: 64 cases (2005-2012). *J Am Vet Med Assoc.* 2015;247(7):786-792. doi:10.2460/javma.247.7.786
6. Kuntz CA, Asselin TL, Dernel WS, Powers BE, Straw RC, Withrow SJ. Limb salvage surgery for osteosarcoma of the proximal humerus: outcome in 17 dogs. *Vet Surg.* 1998;27(5):417-422. doi:10.1111/j.1532-950X.1998.tb00150.x
7. Liptak JM, Dernel WS, Lascelles BDX, et al. Intraoperative extracorporeal irradiation for limb sparing in 13 dogs. *Vet Surg.* 2004;33(5):446-456. doi:10.1111/j.1532-950x.2004.04068.x
8. Kubicek L, Vanderhart D, Wirth K, et al. Association between computed tomographic characteristics and fractures following stereotactic radiosurgery in dogs with appendicular osteosarcoma: stereotactic radiosurgery in dogs with appendicular osteosarcoma. *Vet Radiol Ultrasound.* 2016;57(3):321-330. doi:10.1111/vru.12351
9. Martin TW, Griffin L, Custis J, et al. Outcome and prognosis for canine appendicular osteosarcoma treated with stereotactic body radiation therapy in 123 dogs. *Vet Comp Oncol.* 2021;19(2):284-294. doi:10.1111/vco.12674
10. Dekker TJ, Steele JR, Federer AE, Hamid KS, Adams SB. Use of patient-specific 3D-printed titanium implants for complex foot and ankle limb salvage, deformity correction, and arthrodesis procedures. *Foot Ankle Int.* 2018;39(8):916-921. doi:10.1177/1071100718770133
11. Fan H, Fu J, Li X, et al. Implantation of customized 3-D printed titanium prosthesis in limb salvage surgery: a case series and review of the literature. *World J Surg Onc.* 2015;13(1):308. doi:10.1186/s12957-015-0723-2
12. Timercan A, Brailovski V, Petit Y, Lussier B, Séguin B. Personalized 3D-printed endoprostheses for limb sparing in dogs: modeling and in vitro testing. *Med Eng Phys.* 2019;71:17-29. doi:10.1016/j.medengphy.2019.07.005
13. Séguin B, Pinard C, Lussier B, et al. Limb-sparing in dogs using patient-specific, three-dimensional-printed endoprosthesis for distal radial osteosarcoma: a pilot study. *Vet Comp Onc.* 2020;18(1):92-104. doi:10.1111/vco.12515
14. Shahar R, Milgram J. Morphometric and anatomic study of the forelimb of the dog. *J Morphol.* 2005;263(1):107-117. doi:10.1002/jmor.10295
15. Russell WMS, Burch RL. *The Principles of Humane Experimental Technique.* Special edition. [Nachdr. der Ausg.] Universities Federation for Animal Welfare; 1992.
16. Laflamme D. Development and validation of a body condition score system for dogs. *Canine Practice.* 1997;22(4):10-15.
17. The World Small Animal Veterinary Association. Muscle condition score charts for dogs and cats; 2018. <https://wsava.org/wp-content/uploads/2020/01/Muscle-Condition-Score-Chart-for-Dogs.pdf>
18. Araújo JF, Rodrigues FB, Abadia FG, et al. Electromyographic analysis of the gait cycle phases of boxer dogs. *Arq Bras Med Vet Zootec.* 2016;68(4):931-937. doi:10.1590/1678-4162-8770
19. Feeney LC, Lin CF, Marcellin-Little DJ, Tate AR, Queen RM, Yu B. Validation of two-dimensional kinematic analysis of walk and sit-to-stand motions in dogs. *American Journal of Veterinary Research.* 2007;68(3):277-282. doi:10.2460/ajvr.68.3.277
20. Hottinger HA, DeCamp CE, Olivier NB, Hauptman JG, Soutas-Little RW. Noninvasive kinematic analysis of the walk in healthy large-breed dogs. *Am J Vet Res.* 1996;57(3):381-388.
21. Le Bras LA, Timercan A, Llido M, et al. Personalized endoprostheses for the proximal humerus and scapulo-humeral joint in dogs: biomechanical study of the muscles' contributions during locomotion. *PLoS ONE.* 2022;17(1):e0262863. doi:10.1371/journal.pone.0262863
22. Lussier B, Flanders JA, Erb HN. The effect of unilateral arytenoid lateralization on rima glottidis area in canine cadaver larynges. *Vet Surg.* 1996;25(2):121-126. doi:10.1111/j.1532-950X.1996.tb01387.x
23. Demaria M, Stanley BJ, Hauptman JG, et al. Effects of negative pressure wound therapy on healing of open wounds in dogs: effects of negative pressure wound therapy on healing of open wounds. *Vet Surg.* 2011;40(6):658-669. doi:10.1111/j.1532-950X.2011.00849.x
24. Koo TK, Li MY. A guideline of selecting and reporting intraclass correlation coefficients for reliability research. *J Chiropr Med.* 2016;15(2):155-163. doi:10.1016/j.jcm.2016.02.012
25. Méndez J, Keys A. Density and composition of mammalian muscle. *Metab Clin Exp.* 1960;9:184-188.
26. Chincisan A, Tecante K, Becker M, Magnenat-Thalmann N, Hurschler C, Choi HF. A computational approach to calculate personalized pennation angle based on MRI: effect on motion analysis. *Int J CARS.* 2016;11(5):683-693. doi:10.1007/s11548-015-1251-9
27. Fukunaga T, Roy RR, Shellock FG, et al. Physiological cross-sectional area of human leg muscles based on magnetic resonance imaging. *J Orthop Res.* 1992;10(6):926-934. doi:10.1002/jor.1100100623
28. Hornby NL, Drees R, Hannon R, Chang R, Wells DJ, Piercy RJ. Musculoskeletal magnetic resonance imaging in the DE50-MD dog model of Duchenne muscular dystrophy. *Neuromuscul Dis.* 2021;31(8):736-751. doi:10.1016/j.nmd.2021.05.010
29. Williams SB, Wilson AM, Daynes J, Peckham K, Payne RC. Functional anatomy and muscle moment arms of the thoracic limb of an elite sprinting athlete: the racing greyhound (*Canis familiaris*). *J Anat.* 2008;213(4):373-382. doi:10.1111/j.1469-7580.2008.00962.x
30. Arnold EM, Hamner SR, Seth A, Millard M, Delp SL. How muscle fiber lengths and velocities affect muscle force generation as humans walk and run at different speeds. *J Exp Biol.* 2013;216(Pt 11):2150-2160. doi:10.1242/jeb.075697
31. Allen PD, Barclay JK. The mechanical properties of in situ canine skeletal muscle. *Front Physiol.* 2022;13:862189. doi:10.3389/fphys.2022.862189
32. Binder MD, Hirokawa N, Windhorst U, eds. *Encyclopedia of Neuroscience.* Springer; 2009.
33. Dries B, Jonkers I, Dingemans W, et al. Musculoskeletal modelling in dogs: challenges and future perspectives. *Vet Comp Orthop Traumatol.* 2016;29(03):181-187. doi:10.3415/VCOT-15-08-0133
34. Chleboun GS, France AR, Crill MT, Braddock HK, Howell JN. In vivo measurement of fascicle length and pennation angle of the human biceps femoris muscle. *Cells Tissues Organs.* 2001;169(4):401-409. doi:10.1159/000047908